Development of a chopper spectrometer at KENS

M. Arai, M. Kohgi, M. Itoh*, H. Iwasa**, N. Watanabe, S. Ikeda, and Y. Endoh**
National Laboratory for High Energy Physics
Oho-Machi, Tsukuba-gun
Ibaraki-Ken, 305
JAPAN
*Department of Physics, Tohoku University
**Department of Engineering, Hokkaido University

1. Introduction

A direct geometry chopper spectrometer combined with an advanced pulsed neutron source has a promising feasibility for its wide accessible dynamic range in Q-ω space and for the applicable various fields of high energy magnetic excitations, molecular dynamics and dynamics of liquids and glasses . The recent scientific requirements of measuring high energy excitations caused the decision to build a chopper spectrometer at KENS.

The development of a sophisticated magnetic bearing made it possible to realize a short chopper burst, due to the high speed revolution, as narrow as the neutron pulse width from a moderator in the epithermal neutron region, providing higher momentum and energy resolution with less sacrifice in intensity.

In this report we discuss a spectrometer called INC, which is under construction at KENS, aiming at neutron scattering with an energy transfer from 20 to 1000meV and a momentum transfer from 0.3 to 40Å^{-1}.

2. Design Performance

INC was installed at beam hole H-6, which views a polyethylene moderator at room temperature. This beam line has the widest and longest available space, so that INC can perform at its highest ability by arranging the detector arrays at a wide scattering angle. However, the flight path of 7m from the bulk shield with 4m thick was the most important restriction for designing the spectrometer. We tried to find optimal parameters to achieve better performance under this restriction. We adopted a horizontal layout rather than a vertical one, and took the parameters L1=7m, the distance between the moderator and the monochromating chopper, L2=1.3 or 2.5m, between the sample and the detector, and L3=1m, between the chopper and the sample. (L2 is 2.5m for the scattering angle 5°-25° for the lefthand side detector bank and 5° - 40° for the righthand side detector bank from the downstream point of view, while 1.3m for 40° - 130°.) These parameters satisfy most of our required performance as discussed below.

2.1. Accessible Range in Q-ω Space

The detectors cover the scattering angle from 5° to 130° and give a wide accessible range in Q-ω Space. Figure 1 shows the accessible Q-ω space at the scattering angles of 5°, 11°, 25°, 40°, 80° and 130° with the incident energies of 100, 400 and 1000meV. As it is well known, due to the kinematic constraint of neutrons, small angle scattering with high energy neutrons is indispensable in measuring the scattering with high energy transfer at smaller Q, which is especially important in high energy magnetic excitations.

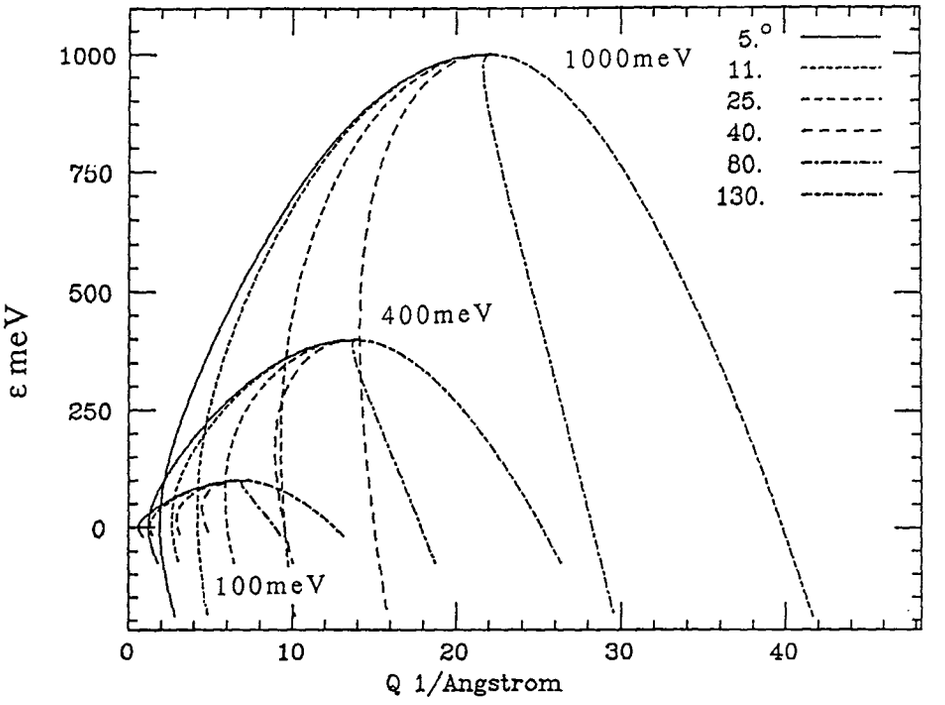

Fig. 1 The Q-ω space accessible with scattering angles of 5°, 11°, 25°, 40°, 80° and 130° for the incident energies of 100, 400, and 1000 meV.

2.2. Resolutions

The energy resolution is essentially determined by two dispersive parts of R1 and R2 due to the chopper opening time width and the neutron burst pulse width at the moderator, as discribed below, and can be expressed in a good approximation as[1],

$$\frac{\Delta\varepsilon}{E_i} = [\{2R_1[1+\frac{L_1+L_3}{L_2}(1-\frac{\varepsilon}{E_i})^{3/2}]\}^2 + \{2R_2[1+\frac{L_3}{L_2}(1-\frac{\varepsilon}{E_i})^{3/2}]\}^2]^{1/2} .$$

Then the momentum resolution is described using the energy resolution as,

$$\frac{\Delta Q}{Q} = \frac{2mE_i}{\hbar^2 Q^2}\left\{ \frac{E_i}{4E_f}\left(\cos(\Phi_0) - \sqrt{\frac{E_f}{E_i}}\right)^2\left(\frac{\Delta\varepsilon}{E_i}\right)^2 + \frac{E_f}{E_i}\sin^2(\Phi_0)\,\Delta\Phi^2 \right\}^{1/2} ,$$

where

$$R_1=\Delta t_{ch}/t_{ch},\ R_2=\Delta t_m/t_{ch} = \delta_m/L_1,\ \Delta t_{ch}=\frac{W}{2v_p}P(u),$$

$P(u)=1+\frac{u}{4}$ for $0<u<0.8$

$P(u)=2+u-(4u-u^2)^{1/2}$ for $0.8<u<2$

$P(u)=u$ for $2<u$

$$u=\frac{W_{mnet}}{L_1}\Big/\frac{W}{D}$$

$$W_{mnet} = W_m\left(\cos(\alpha) - \frac{2\pi L_1 f \sin(\alpha)}{v_0}\right) .$$

The notations used in the above equations are defined below, and shown in Fig.2.

Δt_m	: neutron pulse width
δ_m	: moderator effective thickness
α	: moderator rotation angle
W_m	: moderator width
L_1	: flight path length from the moderator to the chopper
L_2	: flight path length from the sample to the detector
L_3	: flight path length from the chopper to the sample
D	: chopper rotor diameter (assumed to be 10cm)
W	: chopper rotor slit width
t_{ch}	: time of flight at the chopper
Δt_{ch}	: chopper burst time width
f	: revolution frequency of the chopper (assumed to be 600Hz)
v_p	: chopper peripheral speed ($v_p=\pi Df$)
Φ_0	: scattering angle
$\Delta\Phi$	: angular ambiguity by a detector (detector diameter 2.5cm)
v_0	: velocity of incident neutrons
E_i	: incident energy of neutrons
E_f	: final energy of neutrons
ε	: energy transfer
$\Delta\varepsilon$	: ambiguity in energy
k_i	: wave number of incident neutrons
Q	: momentum transfer
ΔQ	: ambiguity in momentum

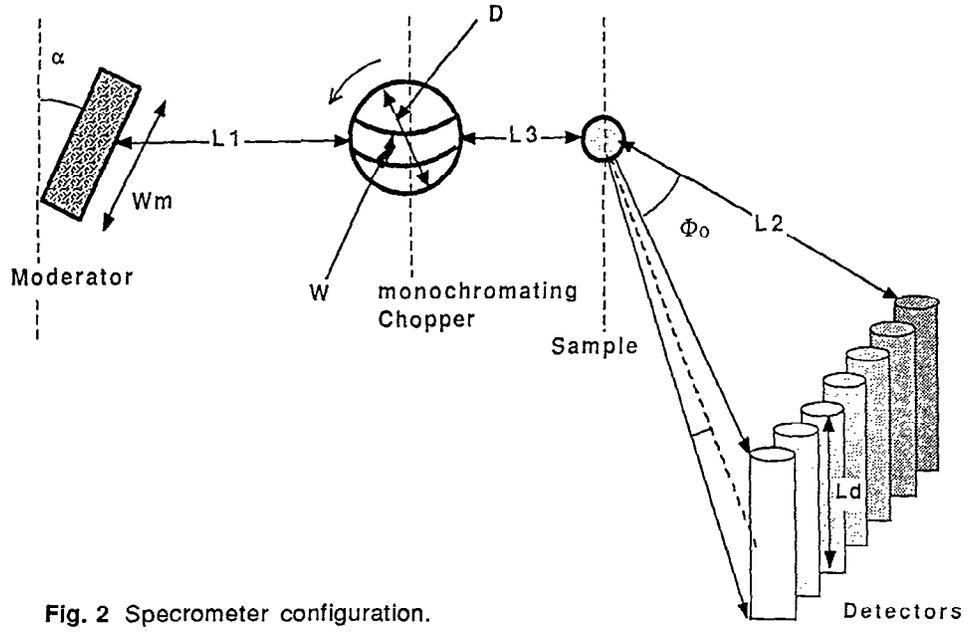

Fig. 2 Specrometer configuration.

For the room temperature moderator in KENS, a neutron pulse width of $\Delta t_m \approx 1.5/\sqrt{E\ [eV]}$ μs is a good approximation in the epithermal neutron range above 250meV, which gives 2.1cm for δ_m , but becomes longer with an asymmetric long tail below 250meV. For example, it is about 10μs at E_i=100meV. The moderator has angle clockwise by 15° to the H-6 beam line, and this configuration gives the optimal time focusing for 500meV. The moderator width W_m is 8cm. The slit width W of the chopper rotor is determined from $\Delta t_{ch} = W/v_p$, with the optimizing condition $\Delta t_{ch} = \Delta t_m$. For example at the incident energy of 300meV, the slit width becomes 0.10cm.

In Fig.3 the energy resolution $\Delta\varepsilon/E_i$ is plotted as a function of ε/E_i. The solid line is for L_2=2.5m, and the upper broken line is for L_2=1.3m. The resolution of HET(high resolution chopper spectrometer at ISIS, RAL) is also plotted as a reference.

Figure 4 shows ΔQ/Q at an ε of $0.2E_i$, $0.4E_i$, $0.6E_i$ and $0.8E_i$ as a function of Q/k_i. The discontinuities at Q/k_i=0.7 correspond to Φ=40°, where L_2 changes from 2.5m to 1.3m.

2.3. Required Resolution

Here we do calculations using actual scientific examples to estimate the feasibility with the designed resolutions.

i) High Energy Magnetic Excitations

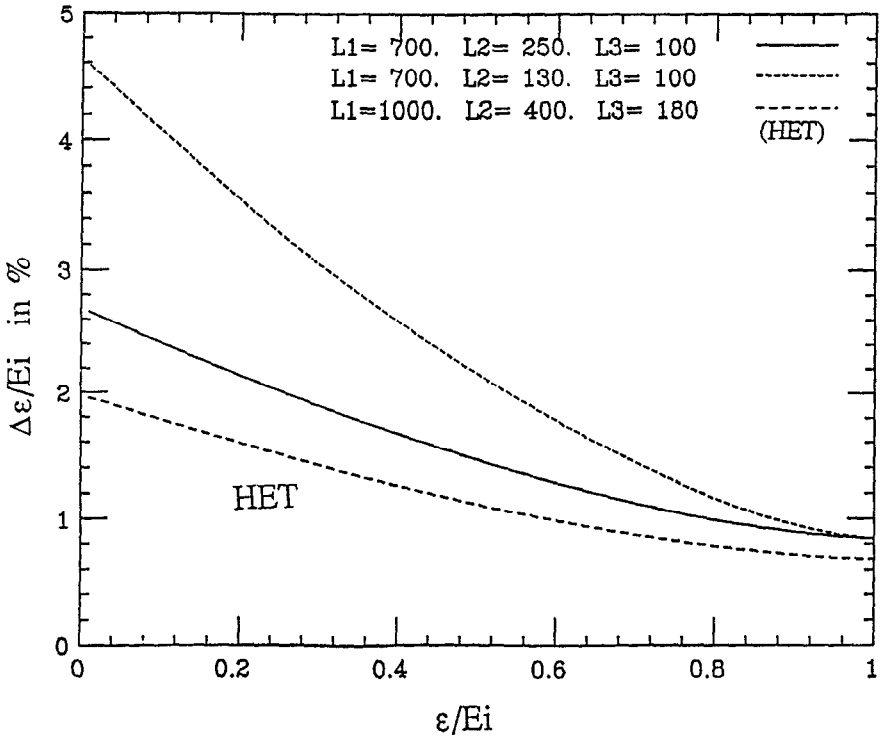

Fig. 3 The energy resolution $\Delta\varepsilon/E_i$ as a finction of ε/E_i. The solid line is L_2 = 2.5 m and upper broken line is L_2 = 1.3 m. The resolution of HET is also plotted as a reference (L_1 = 10, L_2 = 4 and L_3 = 1.8 m).

We consider the crystal field splitting in UO_2 demonstrated by HET[2]. They observed excitations around 150meV with FWHM about 6meV. Now we suppose E_i = 250meV and ε=150meV with Q < 4.5A^{-1}. For this condition the scattering angle Φ <12° is required, and the result is shown in the table below. We can resolve those excitations by a close shave.

Ei	Φ	L2	ε	Δε(calc.)	FWHM(obs.)
250meV	<12°	2.5m	150meV	3meV	6meV

ii) S(Q,ω) of glassy materials

We examine the following extreme examples, although glassy materials in general do not have sharp structure in Q-ω space[3].

SiS_2 glass has an exceptionally sharp excitation as measured in the Raman spectrum at 420cm^{-1} (52meV) with FWHM ≈ 20cm^{-1} (2.4meV) [4] corresponding to the A1 mode. When E_i =100meV, the resolutions are as follows.

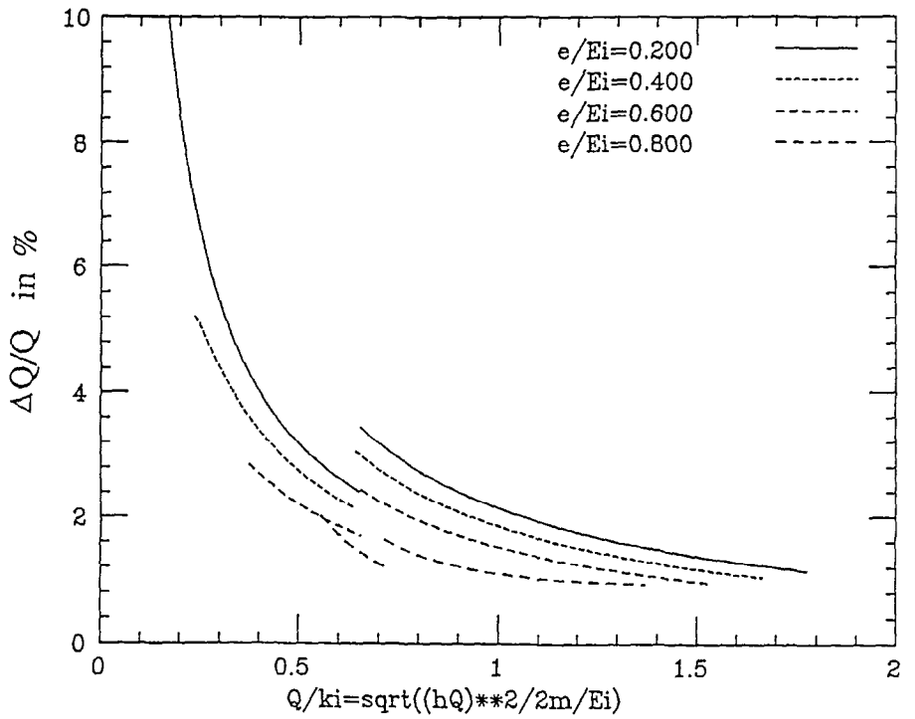

Fig. 4 The momentum resolution ΔQ/Q at e of 0.2 E_i, 0.4 E_i, 0.6 E_i and 0.8 E_i as a function of Q/k_i. The discontinuitites at Q/k_i = 0.7 correspond to the scattering angle $\phi \approx 40°$, where L_2 changes from 2.5 m to 1.3 m.

Ei	L2	ε	Δε(calc.)	FWHM(obs.)
100meV	1.3m	52meV	4.0meV	2.4meV
100meV	2.5m	52	2.8	2.4

The energy resolution Δε for L_2 = 2.5m is just comparable to the natural width of the excitation.

In some glasses[5], there is a first sharp diffraction peak (FSDP) in S(Q) at around 1 A^{-1} with FWHM ≈ 0.2 A^{-1}. When we take E_i=100meV, although this condition is not optimal for measuring elastic scattering at Q = 1 A^{-1}, the momentum resolution ΔQ is again comparable to the FWHM of the FSDP as shown in the table below. From the considerations above, we believe that the resolution of INC are reasonable for usual case.

Ei	Φ	L2	Q	ΔQ(calc.)	FWHM(obs.)
100 meV	8°	2.5m	1.0A^{-1}	0.15^{-1}	0.2^{-1}

3. Chopper System

3.1. Monochromating Chopper and Background Suppression Chopper

A chopper system is supplied from RAL as a part of the UK-Japan collaboration. The chopper is equipped with a magnetic bearing system developed at KFA, Jülich[6]. The chopper is almost the same as that of MARI (multi-angle rotor instrument at ISIS). The rotor can be spun at 600Hz with ±0.2μs phase ambiguity for fixed frequency operation, and is designed to rotate clockwise when viewed from the top in order to realize time focusing. We will have four rotors with different slit packages, which are optimized to E_i= 50, 100, 200 and 500meV. The beam aperture of the chopper is 6x6cm^2.

In order to suppress delayed fast neutrons from the uranium target as well as fast burst neutrons, a background suppression chopper is indispensable for INC. We are developing a mechanical chopper system for this purpose.

3.2. Phasing

In order to achieve the required resolution, the chopper rotor must be phased accurately with the accelerator having a time ambiguity of about ±5μs in successive beam extractions. We have developed electronics to solve this problem.[7] There is an acceptable time band for the extraction of the proton beam from the Booster synchrotron of about ±50μs centered at the peak magnetic field. Within the acceptable band, the beam can be extracted according to a request signal from the chopper. Otherwise, the beam is extracted automatically at the end of the band. Figure 5 shows typical results of the phasing experiment using the Harwell Mk VIII rotor spinning head at a rotor revolution speed of 500rev/s. In the figure the distribution of the extraction time after request signal is plotted. The results show that the beam extraction time is phased to the request signal with a time ambiguity of ±0.4μs and a duty factor of 99%. These values are sufficient for practical operation.

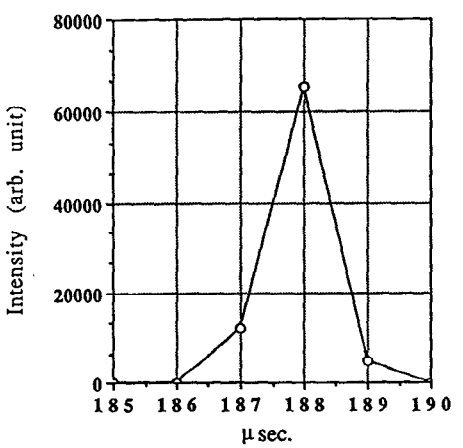

Fig. 5 Typical results of a phasing experiment using Harwell Mk VIII rotor spinning head at a rotor revolution speed of 500 rev/s. The distribution of the extraction time after request signal is plotted.

4. Collimator System

The design of a collimator system was essentially based on the ray diagram consideration[8]. The collimator system consists of two parts. The inner collimator in the bulk shield and the outer collimator between the two choppers consist of sintered B_4C, steel and borated resin (boric-acid 40%, polyethylene-beads 40%, epoxy-adhesive 20% in weight) making an image 6x6cm^2 at the sample position. They were designed so that the iron soften fast neutron spectrum, the hydrogenous compound slows down neutrons to be absorbed by the boron, and the scattered neutrons are captured by B_4C scraper projecting inward in the collimator. Figure 6 shows the details of the collimators.

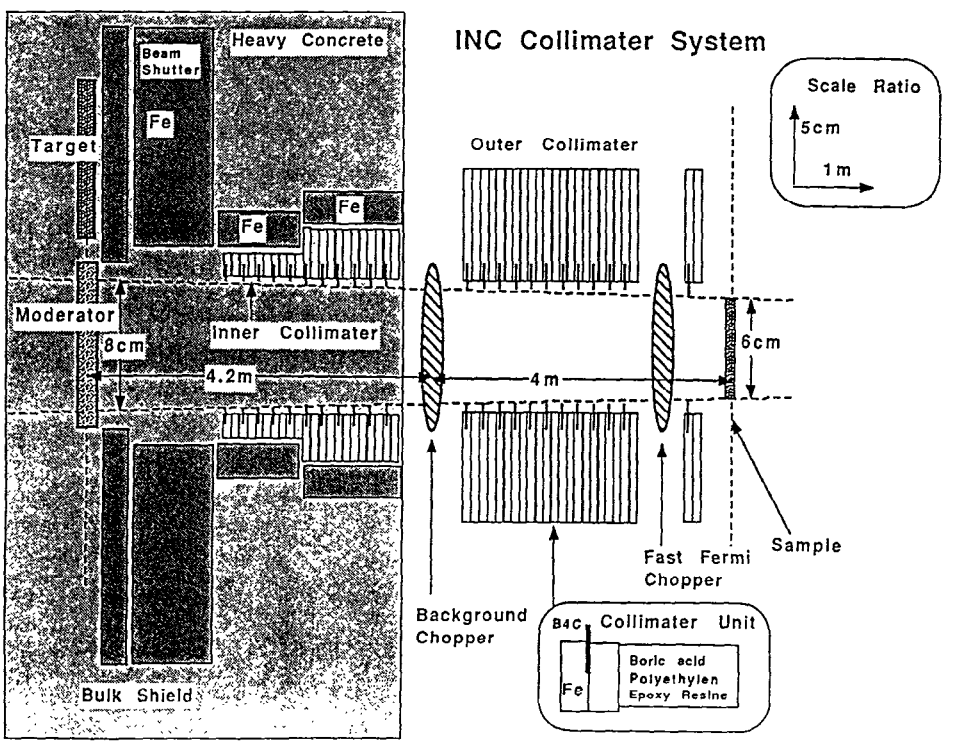

Fig. 6 Details of the collimators. The inner collimator in the bulk shield and the outer collimator between two choppers consist of sintered B_4C, steel and borated resin.

5. Spectrometer

The spectrometer shield enclosing the scattering chamber is mainly made of borated resin (boric-acid polyethylene-beads epoxy-adhesive combination, 45, 45, 10% in weight) 30 - 40cm thick, and partly made of ordinary concrete 30 - 50cm thick. The thickness of these shields was determined by dose measurements under

actual conditions. The shield has a shield door for access to the detectors, and there is a sliding overhead shield for access to the sample.

Figures 7 (a) and (b) show the layout of INC. The scattering chamber consists of two parts; a sample chamber (high vacuum) and a detector chamber (low vacuum). They are separated by a thin aluminum window 0.1mm thick. The detector chamber has 13 detector-windows of aluminum plates 2mm thick. The low angle bank has a flight path length of 2.5m with six-fold detector arrays covering scattering angles from 5° to 11°, which can accommodate 80 detectors (6", 8", 10" and 12" in length,1" in diameter). The medium angle bank consists of 50 detectors (12" in length, 1" in diameter) in single detector arrays, which extend from 11° to 25° at the lefthand side and from 11° to 40° at the righthand side from the downstream point of view. The high angle bank has a flight path of 1.3m, covering scattering angles from 40° to 130°, and can accommodate up to 80 detectors (12" in length, 1" in diameter). In order to cover the angles between the detector banks, there are insertion detector banks in the detector chamber.

The inside of the detector chamber is completely covered by B_4C resin tiles 10mm thick, so that the detectors see only the sample.

6. Data Acquisition System

6.1. Compact Charge-Sensitive Amplifier

We have developed low-cost high-performance charge-sensitive amplifier for multi-detector use[9], which has excellent performance of very low noise with very high counting rate. The amplifier includes a charge-sensitive preamplifier, a pulse shaping amplifier and a discriminator. The size is very compact and is $3 \times 7 \times 10cm^3$. This made it possible to make 200 detectors for INC at a low cost.

6.2. Data Acquisition Electronics

We have developed new data acquisition electronics. The time boundary of the time analyzer can be set in arbitrary way by computer to minimize the time resolution to fit with the other contributions such as neutron burst pulse width and chopper burst width, and can be used very flexibly. The details are described in Ref. 10.

7. Discussions

7.1. Intensity and Background

Here we show the estimated counting rate from U^{4+} (UO_2) in the INC, comparing with the measured background level and the results from the HET[2].

The cross section for crystal field splitting averaged over all direction is given by[11]

$$\left\langle \frac{d^2\sigma}{d\Omega d\varepsilon} \right\rangle = r_0 \frac{k_f}{k_i} P_n \{ a j_0^2 + b j_0 j_2 + c j_2^2 + \ldots \} \delta(\varepsilon - E_{n'} + E_n) .$$

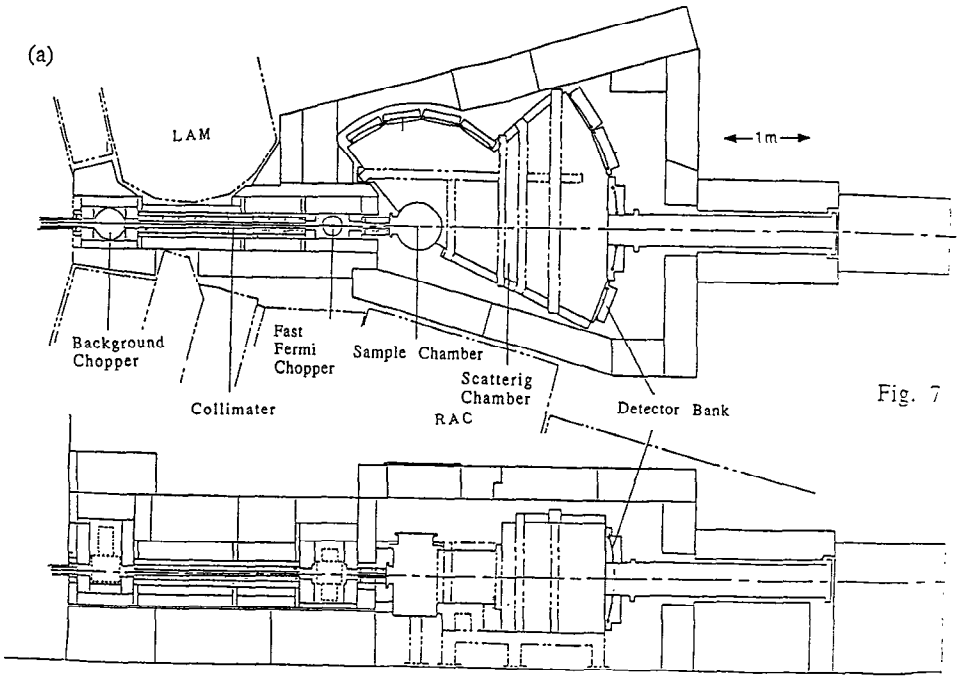

Fig. 7

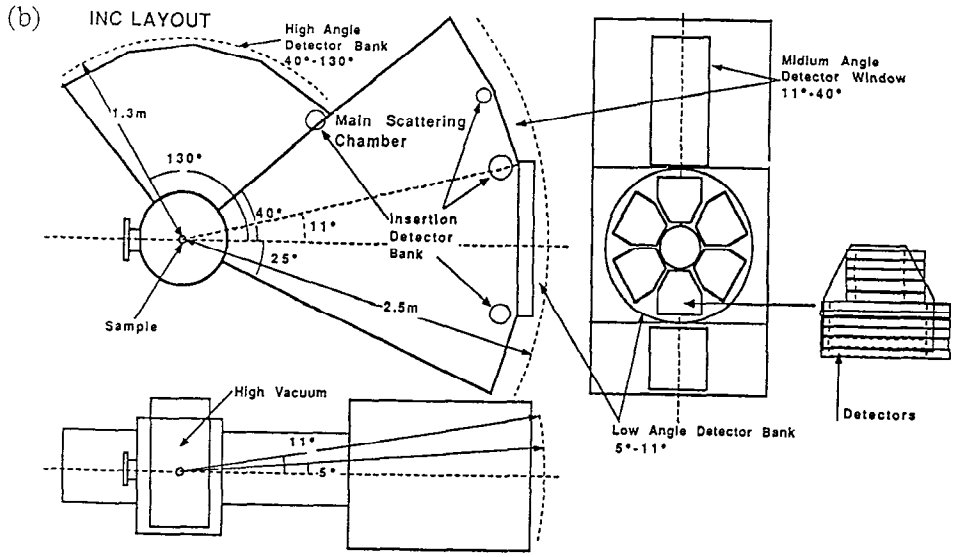

Fig. 7 Layout of the INC.

Here, j_k is the spherical Bessel function of order k. We consider the case of the Γ_5 -> Γ_3 transition, i.e. from the ground level (n=5) to the first excitation level (n'=3) with ε=180meV. P_5 is product of the degeneracy and the population factor, which is about 1/3. a is the matrix element for the transition, and is 1.28. r_0 is $(\frac{\gamma e^2}{m_e c})^2 = 0.29 \times 10^{-24}$. In case that the total momentum is a good quantum number, the zeroth Bessel function is dominant and the cross section can be written by

$$\left\langle \frac{d^2\sigma}{d\Omega d\varepsilon} \right\rangle = r_0 \frac{k_f}{k_i} P_5 \, a j_0^2 \; \delta(\varepsilon - E_5 + E_3) .$$

We take E_i=300meV (k_i=12.2A^{-1}), E_f=120meV and ε=180meV. The cross section at Q=4.5A^{-1} (measured by the 5° detector) with j_0 = 0.6 is

$$\left\langle \frac{d^2\sigma}{d\Omega d\varepsilon} \right\rangle = (-0.54 \times 10^{-12})^2 \; 1/3 \; \sqrt{E_f/E_i} \times 1.28 \times 0.6^2 \; \delta(\varepsilon - E_5 + E_3)$$
$$= 0.0256 \times 10^{-24} \, \delta(\varepsilon - E_5 + E_3) \quad [cm^2/meV/str]$$

Then the counting rate (integrated intensity of I(ε)) at a detector is

$$\int I(\varepsilon) \, d\varepsilon = \int d\varepsilon \; i(E_i) \; N \left\langle \frac{d^2\sigma}{d\Omega d\varepsilon} \right\rangle T(E_i) \; f(E_f) \; P \; C \; d\Omega$$
$$= 15.6 \; [n/day/detector/\mu A]$$

The flux intensity at the sample position $i(E_i)$ is expressed as,

$$i(E_i) = r/(L_1+L_3)^2 \; \Delta\varepsilon/E_i \qquad [n/cm^2/p].$$

The values used are as follows,

- the intensity of neutrons from a moderator per steradian per eV at E_i per proton expressed by r is

$$r = 1.0 \times 10^{-2} \times \left(\frac{E_i(0.3eV)}{E_i(1eV)} \right)^{-0.88} \quad [n/str/eV/p] \quad \text{for } E_i = 300meV.$$

- $\Delta\varepsilon/E_i$=1.3% at 180meV , i.e. $\Delta\varepsilon$=3.9meV or Δt=8μs at t=516μs.
- sample amount is N=0.3mol (1.8 x10^{23} U atoms) assuming 10% scatterer and the beam size of 60(wide) x 60(long) x 2(thick)mm^3.
- $T(E_i)$ is the transmission of the chopper, typically 0.5.
- $f(E_f)$ is the detector efficiency, 0.8.
- P is the number of proton pulses in a day, 1224 x 10^3 pulses/day.
- C is the number of protons per proton pulse per μA, 3.1*10^{11} ppp/μA.
- $d\Omega$ is the solid angle subtended by a detector (2.5x30cm^2) at the 2.5m position, 1.2 * 10^{-3} str.

If the counting rate estimated above is spread over 20 meV (50μs), we have **0.33**cnt/day/μs/detector/μA. This value should be compared with the background counts, **0.034** cnt/day/μs/detector/μA, which was obtained with a reference detector surrounded by 2cm thick B_4C resin and 30cm thick boric acid.

The counting rates from UO_2 measured in the HET were scaled by the parameters of KENS, and are 0.18 for the signal and 0.056 for the background. The counting rate 0.33 estimated above shows fairly good agreement with the scaled value of HET measurement. The thickness of the constructed shield seems to be good enough for distinguishing the signal from the background.

7.2. Counting Rate

It turns out that the performances of INC satisfy most of the requirements for the targeted scientific fields. The counting rate per unit solid angle of INC, $I(\varepsilon)_{INC}$, is compared in a Table below with HET and MARI,

	L_1 (m)	L_3 (m)	L_2(m)	P(μA)	M	A(cm^2)	$I(\varepsilon)/I(\varepsilon)_{INC}$
INC	7.2	1	2.5	8	2	6 x 6	**1**
HET	10	1.8	4	200	1	5 x 5	**1.2**
MARI	10	1	4	200	1	6 x 6	**2.0**

where $I(\varepsilon) \approx 1/(L_1+L_3)^2/L_2^2\ \Delta\varepsilon/E_i \times P \times M \times A$. P is the proton current, M is the target-moderator coupling factor, A is the sample area and $I(\varepsilon)/I(\varepsilon)_{INC}$ is the ratio of the expected intensity at a detector for the spectrometer to that of INC.

As we see here, the counting rate per unit area at the detector position in INC has encouraging value even compared with that in HET and MARI in spite of the lower proton current at KENS. Therefore INC could produce reasonable scientific output with a slightly lower resolution.

Acknowledgements

We acknowledge Dr. C.K. Loong for the helpful advice in the early stage of the design work. We also acknowledge Dr. A.D. Taylor, R. Ward and Mr. T.J.L. Jones for stimulating discussions on the chopper spectrometer and the chopper system.

References

1) C. J. Carlile, A. D. Taylor and W. G. Williams; MARS - A Multi-Angle Rotor Spectrometer for SNS, RAL-85-052.
2) A. D. Taylor, B. C. Boland, Z. A. Bowden and T. J. L. Jones; HET The High Energy Inelastic Spectrometer at ISIS, RAL-87-012.
3) M. Arai, D. L. Price, S. Susman, K. J. Volin and U. Walter, Phys. Rev. B**37**, 1988, 4240.
4) M. Tenhover, M. A. Hazle and R. K. Grasselli, Phys. Rev. Lett. **51**,1983, 404.
5) R. W. Johnson, D. L. Price, S. Susman, M. Arai, T. I. Morrison and G. K. Shenoy J. Non-Cryst. Solids **75**, 1986, 57

6) T. J. L. Jones, J. H. Parker, I. Davidson, K. Boden and J. K. Fremery, Proc. ICANS VIII 1985 at RAL, UK, p707.
7) M. Arai, M. Kohgi, Y. Arakida and M. Hosoda, KENS report VI 1987 KEK p68.
8) W. S. Howells, Proc. ICNAS-IV 1980 at KEK, Japan, p359
9) M. Arai, M. Hosoda and M. Kohgi, unpublished
10) M. Arai, M. Furusaka, M.W. Johnson and S. Satoh, KENS report VII 1988 KEK p24.
11) S. W. Lovesey; Theory of neutron scattering from condensed matter. 1984, Vol. 2, p242.